THE DEATHS OF STELLAR DYNAMOS: DIGGING IN THE MAGNETIC GRAVEYARD FOR OLD COLD CORONAE

Abstract: Sun-like stars exhibit three distinct phases of magnetic evolution. In the saturated regime, the X-ray luminosity is independent of the rapid rotation. For slightly older stars in the unsaturated regime, the X-ray luminosity declines in tandem with rotation. Recent observational evidence suggests that near the middle of their main-sequence lifetimes, stars may enter a third regime in which rotation remains nearly constant while magnetic activity continues to decline. We propose to measure X-ray luminosities for three stars with a range of spectral types and metallicities, to identify the signature of this third regime in the old cold coronae of stars that appear to have shut down their global dynamos. We will use previous observations to help constrain the coronal temperatures.

Science Justification

Nearly half a century ago, Skumanich (1972) observed that both the rotation rate and the magnetic activity of stars decay with a power-law dependence on age. Stars are formed with a range of initial rotation rates, and they gradually lose angular momentum through their magnetized stellar winds, a theory known as magnetic braking. The process is stronger in rapidly rotating stars, which enforces convergence to a single rotation rate at a given mass after roughly 500 Myr in Sun-like stars. The evidence for this scenario relies on studies of rotation in young star clusters at various ages, and until recently the only calibration point for ages beyond 2.5 Gyr was from the Sun.

Observations from the *Kepler* space telescope provided the first opportunity to measure rotation rates for a variety of FGK field stars with ages determined from asteroseismology. The younger stars appeared to obey the Skumanich relation, but the older stars were rotating more quickly than expected. This anomalous rotation becomes significant near the solar age (4–5 Gyr) for G-type stars, but it appears at 2–3 Gyr for hotter F-type stars and at 6–7 Gyr for cooler K-type stars. The dependence on spectral type suggests a connection to the Rossby number ($\mathrm{Ro} \equiv P_{\mathrm{rot}}/\tau_c$), because hotter stars have shallower convection zones with shorter turnover times (τ_c). The *Kepler* observations were reproduced with rotational evolution models that dramatically reduce angular momentum loss beyond a critical Rossby number comparable to the solar value (van Saders et al. 2016).

Ground-based observations of chromospheric activity for the *Kepler* sample revealed a magnetic counterpart to this rotational transition. The critical Rossby number is equivalent to a specific level of chromospheric activity, and the amount of time it takes a star to reach this threshold depends on its spectral type. The shutdown of magnetic braking near the solar activity level appears to decouple rotation and magnetism, locking the surface rotation rate while the chromospheric activity level continues to decrease with age (Metcalfe et al. 2016). The disruption of magnetic braking may arise from a concentration of the global field into smaller spatial scales, possibly due to a change in the differential rotation from a diminishing imprint of Coriolis forces on the convection.

This new picture of rotational and magnetic evolution provides a framework for understanding how stellar activity cycles change over the lifetimes of Sun-like stars. **Figure 1** shows an updated version of a diagram published by Böhm-Vitense (2007). When we color code the points by spectral type and indicate the rotation periods of non-cycling stars along the top, it becomes clear that cycles are no longer observed in stars beyond the critical Rossby number where magnetic braking shuts down. Within this picture, stars that fall between the two sequences, including the Sun and HD 166620 as well as α Cen A, can be understood as dynamos in transition. Considering the evolutionary sequence defined by 18 Sco (4.1 Gyr), α Cen A (5.4 Gyr) and 16 Cyg (7.0 Gyr), the data suggest that a normal cycle on the lower sequence may grow longer across the transition (dashed lines) before disappearing entirely (Metcalfe &

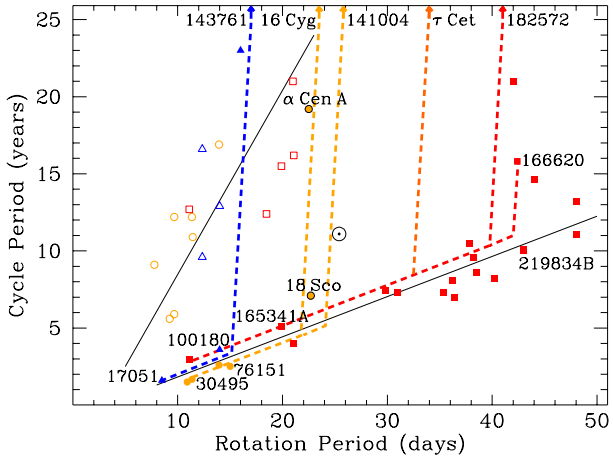

Figure 1: *Relation between rotation and cycle period for two types of dynamos, from shear layers near the surface (open points) and near the base of the convection zone (solid points). Colors indicate spectral type, including F-type (blue triangles), G-type (yellow circles), and K-type stars (red squares). Dashed lines show empirical evolutionary tracks, leading to stars with constant activity (arrows along the top) that appear to have completed the dynamo transition.*

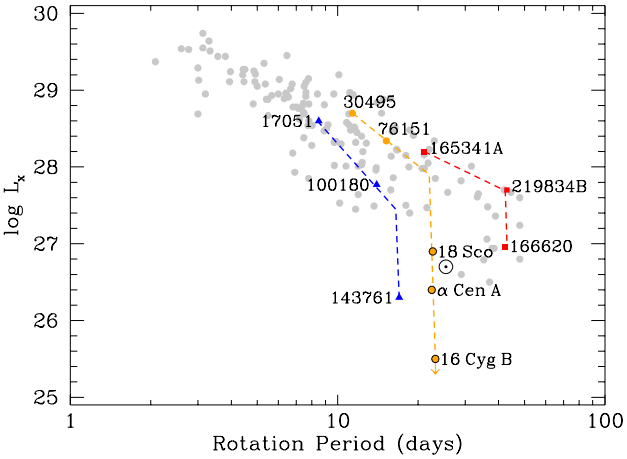

Figure 2: *Relation between rotation and X-ray luminosity near the bottom of the unsaturated regime. Field stars from Wright et al. (2011) are shown as gray points, while selected stars from Figure 1 are shown as colored points. As the cycle grows longer and becomes weaker, the X-ray luminosity shows a corresponding drop, which may be a third regime of magnetic evolution that new X-ray measurements can effectively probe.*

van Saders 2017). The rotation period at the transition is a sensitive function of convection zone depth, so several dashed lines are shown.

The decoupling of rotation and magnetism in middle-aged stars, and the coincident shift in dynamo properties, suggests the possibility of a third regime in magnetic evolution that X-ray measurements can effectively probe. Young rapidly rotating stars in the saturated regime lose angular momentum without a corresponding change in magnetic flux. Intermediate-age stars in the unsaturated regime transition to magnetic topologies that strongly couple the evolution of rotation and activity. In the late stages of their main-sequence lifetimes, stars appear to transition back to a magnetic topology with greater complexity (Garaffo et al. 2018), halting the evolution of rotation while the magnetic flux continues to decrease. **Figure 2** illustrates this mid-life transition for many of the stars that are labeled in Figure 1, showing that the shift in dynamo properties coincides with a sharp drop in X-ray luminosity. This behavior is most apparent in the solar analogs (yellow points), which lead to the recent *Chandra* upper limit for 16 Cyg B (Judge et al. 2017), but additional evidence comes from the hotter star HD 143761 (Judge & Saar 2007) and the cooler star HD 166620 (Wright et al. 2011).

We propose to obtain new measurements of the X-ray luminosity for three stars with a range of spectral types and metallicities, to characterize this mid-life magnetic transition by probing the old cold coronae of stars that appear to have shut down their global dynamos. Our targets are indicated with arrows along the top of Figure 1 at their respective rotation periods, and they will build upon the recent and scheduled *Chandra* measurements of 16 Cyg (PI: Guinan) and τ Cet (PI: Saar). Like these other stars, our targets all have decades-long records of essentially constant chromospheric activity at a low luminosity ($\log R'_{HK} < -5$), suggesting that they are beyond the critical Rossby number where magnetic braking shuts down (Metcalfe & Egeland 2019).

HD 141004 (B−V=0.60, [Fe/H]=+0.09) is an old solar analog, while HD 143761 (B−V=0.60, [Fe/H]=−0.17) is metal-poor, giving it a shallower convection zone like an F-type star. Both of these targets will be observed by the TESS mission for 54 days in early-2020, yielding precise asteroseismic masses and ages. HD 182572 (B−V=0.77, [Fe/H]=+0.39) is cooler and metal-rich, giving it a deeper convection zone like a K-type star. It's rotation period places it near the critical Rossby number for cool stars, but it could also be a more massive subgiant that has slowed to this rotation period as it expanded and cooled. If it is an evolved K-type star, TESS observations for 27 days in mid-2019 are unlikely to detect solar-like oscillations, while an F/G subgiant would almost certainly produce an asteroseismic detection, again yielding the mass and age. The result of our new measurements—along with the data to be obtained for 16 Cyg and τ Cet—will be a decisive test of the late-stage behavior of stellar dynamos, helping to elucidate the mechanism behind the disruption of magnetic braking in middle-aged stars and potentially establishing a third distinct regime in magnetic evolution.

By combining our new HRC-I measurements with previous X-ray observations, from instruments with different response functions, we can constrain the coronal temperatures and the fluxes simultaneously. The 2012 *Chandra* ACIS-S observation of HD 143761 (plotted in Figure 2) detected only 6 X-ray source photons, and the resulting X-ray flux is very uncertain based on both Poisson statistics and the unknown coronal temperature. The reason for the very weak detection is that ACIS is not sensitive to very cool coronal plasma with $\log T < 6.3$. The ratio of HRC-I/ACIS-S counts increases with decreasing temperature. HD 143761 shows essentially constant activity for decades, so the source comparison of HRC-I with the earlier ACIS-S data can provide constraints on the mean coronal temperature. A similar analysis can be completed for HD 141004, which was observed with the *ROSAT* PSPC instrument in 1997. No previous X-ray observations are available for HD 182572, so we will need to assume a coronal temperature that is comparable to one of the other targets. We will also leverage the Cycle 20 measurements of 16 Cyg B and τ Cet to assess the full range of observed coronal temperatures among these non-cycling stars.

Joint HST Observations. We also propose to obtain COS FUV spectra of HD 141004 and HD 182572. HD 143761 already has an archival GHRS spectrum (Judge & Saar 2007; these results will be used in our analysis). All of our targets have archival *IUE* LWR or LWP high spectra which will be sufficient for Mg II fluxes with S/N∼20. These data will permit us to explore the energetic products of "dead dynamos" in several ways, including:

(1) We will survey magnetic heating throughout the sub-coronal atmosphere, from lower chromosphere (Mg II hk; O I 1305 Å), to the upper chromosphere (C II 1335 Å), and transition region (TR; O V 1371 Å, Si IV 1394 Å, C IV 1550 Å), spanning formation temperatures from ∼8,000 K to 130,000 K.

(2) Density sensitive TR lines of O IV] around 1400 Å will be useful to determine densities just below the coronal base.

(3) Results of (1) can be used to compare flux-flux and flux-rotation relations for "dead dynamo" stars with normal cycling dwarfs; how do heating rates differ? In particular, the amount of acoustic heating declines to zero as one rises from the chromosphere to the corona; significant TR or any coronal emission would be evidence for residual magnetic heating in our targets.

(4) Results of (1) can also be compared with stars that appear to be entering Magnetic Grand Minima (MGM), episodes when the cycling dynamo temporarily falters and spots almost vanish (e.g, Saar & Testa 2012). It can be ambiguous whether a non-cycling star is in MGM or has a "dead dynamo". But if a star's cycle amplitude is observed to decay to near zero, its MGM status is clear, since the probability of viewing the exact moment of dynamo "death" (if there is a single moment) is highly unlikely. HD 3651 (Judge & Saar 2007) and HD 4915 (Shah et al. 2018; Cycle 21 proposal) have been proposed as stars potentially entering MGM; how do their outer atmospheres differ, if at all, from our targets?

Table 1: *Target stars together with relevant information for the exposure calculation. Radii are from Valenti & Fischer (2005). Neutral H column densities were computed assuming a local ISM neutral density of 0.07 particles/cm^2. X-ray fluxes correspond to the 0.3-5 keV band.*

Target	Spec. Type	Radius [$R_\odot$]	Distance [pc]	$N_H \times 10^{18}$ [cm^{-2}]	F_X [erg cm^{-2} s^{-1}]	Exp. [ks]	Visibility
HD 141004	G0 V	1.318	11.82	2.6	1.3×10^{-14}	6	2020/01/01–10/03
HD 143761	G0 V	1.317	17.48	3.8	5.8×10^{-15}	12	All year
HD 182572	G7 IV	1.347	14.96	3.2	8.3×10^{-15}	9	2020/02/22–12/10

Technical Feasibility

We base the *Chandra* feasibility on count rate estimates using the most recent version of PIMMS (v4.9a) incorporating Cycle 21 instrument responses, and APEC models of optically-thin, collision-dominated radiative loss appropriate for stellar coronal emission.

Instrument Choice and Count Rates.
There are potentially three instrument choices for this program: ACIS-I, ACIS-S and HRC-I. HRC-S is not considered because its on-axis response is similar to that of HRC-I but with a higher background rate. **Figure 3** illustrates the predicted count rate for the three instruments as a function of isothermal coronal temperature for the most distant of our targets, HD 143761, together with the HRC-I count rate for our other two targets. These estimates assumed a surface X-ray flux of 2×10^{-5} erg cm^{-2} s^{-1}, which is five times lower than the "minimum", solar coronal hole-like, surface flux found for inactive FGK stars in volume-limited *ROSAT* stellar X-ray surveys by Schmitt (1997) and Schmitt & Liefke (2004). Assuming this surface flux provides contingency for the comparatively rare low activity levels of our targets, which may fall below the Schmitt & Liefke limit.

The count rate loci illustrated in Figure 3 demonstrate the difficulties in using the ACIS detector for low activity stars: coronal temperatures are expected to be cooler than those of active stars, and X-ray spectra are too soft for ACIS with its present level of filter contamination. Acquiring the number of counts sufficient for a plasma temperature estimate with ACIS would require very long exposure times.

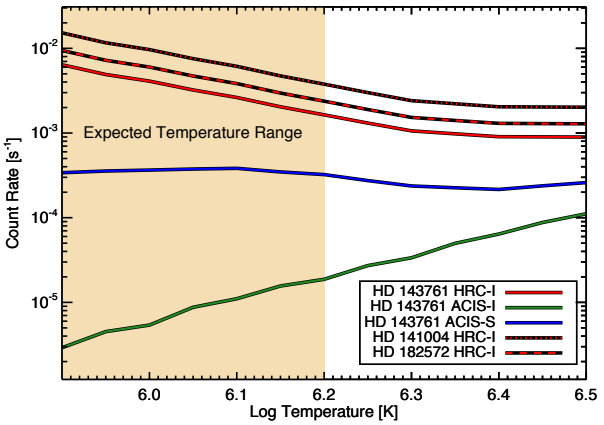

Figure 3: *Predicted source count rates as a function of isothermal plasma temperature computed using PIMMS v4.9a. The expected temperature range of our targets is indicated with the shaded region.*

Instead, HRC-I provides an excellent option for faint, very soft X-ray sources. Our requested exposure times are based on the pessimistic case of a coronal temperature of $\log T = 6.2$, which yields the lowest count rate within the expected range of coronal temperatures characterizing our targets, and for acquisition of 20 counts. The latter, including an HRC-I background rate for a source region of radius 2 arcsec (after filtering) of 3.4×10^{-4} count s^{-1}, yields a signal-to-noise ratio ≥ 4. This provides sufficient leverage to distinguish our target stars within the diagram in Figure 2. Exposure times and other relevant target data are summarized in **Table 1**.

Visibility. *PRoVis* indicates no visibility problems for our targets. Visibility is summarized in Table 1; all pitch angles are below 156° during times of visibility.

Table 2: *Surface fluxes $F_i/10^3$ at the star from HST observations (top two lines) and predictions of the observed fluxes $f_i/10^{-14}$ at the Earth for our proposed targets (bottom two lines).*

Star	[Fe/H]	Radius	Distance	$F_i/10^3$ or $f_i/10^{-14}$ [ergs cm^{-2} s^{-1}]					
		[$R_\odot$]	[pc]	O I	C II	O V	Si IV	O IV]	C IV
τ Cet	−0.36	0.842	3.65	···	···	0.06	···	0.27	···
HD 143761	−0.17	1.317	17.48	7.2	4.7	···	3.3	···	4.8
HD 141004	+0.09	1.318	11.82	4.6	4.5	0.042	2.7	0.21	3.9
HD 182572	+0.39	1.347	14.96	3.0	4.8	0.032	2.3	0.14	3.3

Technical Justification for HST

We wish to detect several FUV emission lines in our targets. Fortunately, similar stars have already been observed with *HST* GHRS; we use surface fluxes in line i, F_i, derived from these data to predict observed fluxes f_i for our targets. For the strongest lines, we scale from the non-cycling star HD 143761 (Judge & Saar 2007); for weaker lines, we scale from averaged intensities $\langle I_i \rangle$ in the nearer non-cycling star τ Cet (Judge et al. 2004; $F_i = \pi \langle I_i \rangle$ from their table). These line surface fluxes F_i (**Table 2**) are scaled by stellar radii (Valenti & Fischer 2005), and distances derived from Gaia. We further correct for metallicity differences between our metal poor "input data" stars (HD 143761 and τ Cet) and our more metal rich targets, following the prescription of Judge & Saar (2007)—scaling by the metallicity difference adjusted by a $\gamma(T_{\rm form})$ factor. For our lines we have $\gamma(T_{\rm form}) = 0.0$, 0.7, 0.4, 0.4, 0.2, and 0.1 for O I, C II, Si IV, C IV, O IV], and O V, respectively (the value for O V is estimated). The resulting predictions of the observed fluxes f_i are given in Table 2.

We note that HD 141004 has a previous *IUE* SWP low observation, but the spectrum is quite low resolution (6 Å), insufficient to separate the Si IV, O IV] blend, and it has low S/N (∼4 in C IV) with O V 1371 Å undetected. Our proposed *HST* observation will vastly improve upon this previous spectrum in both resolution and S/N.

After a 6 minute guide star acquisition, a 3 minute acquisition image (BOA+mirror A) and a 5 minute first exposure setup, we will take a PSA G140L spectrum for the remainder of the orbit (∼40 minutes) to obtain the FUV spectrum. This procedure will then be repeated for the second star, yielding a **total request of 2 orbits**. For the requested 2400 second exposures, 0.5 Å line widths, and average background properties, we obtain S/N per resolution element in the lines >40 in both stars for O I, C II, Si IV, and C IV, plus $S/N_{OV} = 5$ & 7, and $S/N_{OIV]} = 12$ & 15 for HD 182572 & HD 141004, respectively. These S/N are sufficient to accomplish our scientific objectives.

References

Böhm-Vitense, E. 2007, ApJ, 657, 486

Garraffo, C., Drake, J.J., Dotter, A., et al. 2018, ApJ, 862, 90

Judge, P.G., Saar, S.H., Carlsson, M., Ayres, T.R. 2004, ApJ, 609, 392

Judge, P.G., Saar, S.H. 2007, ApJ, 663, 643

Judge, P.G., Egeland, R., Metcalfe, T.S., Guinan, E., Engle, S. 2017, ApJ, 848, 43

Metcalfe, T.S., Egeland, R., van Saders, J. 2016, ApJ Lett., 826, L2

Metcalfe, T.S., van Saders, J. 2017, Sol.Phys., 292, 126

Metcalfe, T.S., Egeland, R. 2019, ApJ, 871, 39

Saar, S.H., Testa, P. 2012, IAU Symp., 286, 335

Schmitt, J. 1997, A&A, 318, 215

Schmitt, J., Liefke, C. 2004, A&A, 417, 651

Shah, S.P., et al. 2018, ApJ Lett., 863, L26

Skumanich, A. 1972, ApJ, 171, 565

Valenti, J.A., Fischer, D.A. 2005, ApJS, 159, 141

van Saders, J.L., Ceillier, T., Metcalfe, T.S., et al. 2016, Nature, 529, 181

Wright, N.J., Drake, J.J., Mamajek, E.E., Henry, G.W. 2011, ApJ, 743, 48